American Welding Society®

SUPPLEMENT TO THE *WELDING JOURNAL*, SEPTEMBER 2022
Sponsored by the American Welding Society

WELDING RESEARCH

Comparison of Stress Relaxation Cracking Susceptibility of Austenitic Stainless Steels

This study shows that the susceptibility of stress relaxation cracking can be determined by the material and strain

BY H.-S. LEE, B.-S. KIM, AND S. I. HONG

Abstract

Coal-fired power plants often have welded joints made up of 347H stainless steel. However, this alloy is known to fail because of stress relaxation cracking. Thus, quantitative evaluation methods are needed as screening measures. In this study, a Gleeble® thermomechanical simulator was implemented in 347H and Super 304H alloy heat-affected zone (HAZ) simulation and stress relaxation testing. In the case of 347H, carbide dissolution in the HAZ reduced the hardness value and promoted grain growth. Alternatively, the respective extent of precipitate dissolution and hardness reduction in the nitrogen-containing Super 304H was relatively small. The stress relaxation tests were performed at a temperature of 700°C (1292°F), which was maintained for up to 70 h. Consequently, all 347H specimens fractured within 32 h. Furthermore, the time to rupture substantially decreased as the strain was increased from 5 to 10% and then to 15%. Additionally, the hardness near the fractured surface increased, and the plastic deformation primarily occurred near the grain boundaries. Conversely, the Super 304H specimens did not fracture during the 70-h testing period, at which time their hardness distribution was observed to still be relatively uniform. These results demonstrate that the susceptibility of stress relaxation cracking can be quantitatively determined according to the material and strain.

Keywords

- Gleeble®
- Stress Relaxation
- Strain-Induced Precipitation Hardening
- Carbide Dissolution
- Heat-Affected Zone (HAZ)
- Strain-Induced Martensite
- Misorientation

Introduction

The high-temperature section of ultrasupercritical boilers that operate at a steam temperature of 600°C (1112°F) is typically made up of austenitic stainless steel such as 347H, Super 304H, or HR3C. However, in the case of 347H, there have been many reports of damage occurring in the heat-affected zones (HAZs) and curved tubes after a relatively short period of operation (i.e., one to two years). Similar cases of damage related to stress relaxation cracking in the curved tubes and HAZs made of 347H have been reported in South Korea and abroad. As a result, there have been numerous studies focused on attempting to identify the cause (Refs. 1–3).

In most cases, the intergranular cracking of the 347H welded joint was observed with the dissolution of niobium carbide and the increase in hardness. The explanation proposed by van Wortel (Ref. 4) and Li et al. (Ref. 5) involves the phenomenon of strain-induced precipitation hardening, wherein fine precipitates formed in the grains and subsequently hardened. Specifically, coarse carbides formed at grain boundaries owing to the fast diffusion rate. This consequently led to deformation as well as the formation of cracks that concentrated at grain boundaries, which began propagating when the stainless steel was exposed to high

https://doi.org/10.29391/2022.101.017

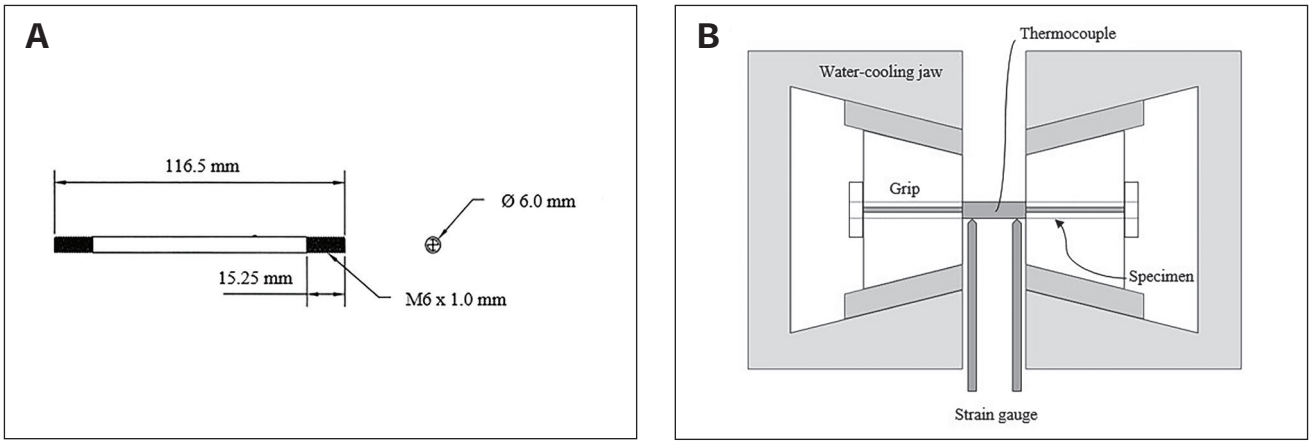

Fig. 1 — A schematic diagram: A — Test specimen; B — Gleeble grips.

Table 1 — Chemical Compositions of 347H and Super 304H Stainless Steel (wt-%)

Specimen	C	Mn	Si	P	S	Ni	Cr	Nb	Cu	N
347H	0.044	1.46	0.164	0.032	0.002	9.18	17.4	0.44	—	—
Super 304H	0.08	0.8	0.19	0.025	0.001	8.8	18.4	0.48	3.0	0.1

temperatures after following deformation induced by cold working and welding.

This cracking phenomenon is not unique to welded zones. It is also known to occur in curved tubes. The American Society of Mechanical Engineers (ASME) standard on boilers and pressure vessels recommends the application of a solution heat treatment to the austenitic tubes if the deformation exceeds 10–20% during bending (Ref. 6). It should be applied according to the steel type and design temperature. The U.S. Electric Power Research Institute (EPRI) recommends a more conservative approach to heat treatment. Taking strain-induced precipitation hardening into consideration, EPRI states that heat treatment should be applied when the amount of deformation exceeds 5% (Refs. 7, 8).

The methods for measuring the susceptibility of stress relaxation cracking can be categorized into two types (Ref. 9). First, there are the Lehigh (Ref. 10), Y-groove (Ref. 11), modified implant (Ref. 12), and British Welding Research Association (BWRA) (Ref. 13) methods, which evaluate crack resistance by analyzing the self-constraint applied during welding. These methods only identify the occurrence of cracks and do not provide quantitative results. Consequently, they are primarily used to evaluate the welding procedure and postheat treatment conditions to prevent stress relaxation cracking. Secondly, there are quantitative evaluation methods (Refs. 14, 15) that employ a thermomechanical simulator, such as a Gleeble® system (Dynamic System Inc.), to simulate the microstructure of the HAZ and evaluate the rupture time or elongation following strain application. These methods have been deemed to be reliable because they can simulate various welding processes, residual stresses, and heat treatments.

This study was designed with the following aims: 1) Employ a Gleeble thermomechanical simulator to apply temperature and strain history data that can be obtained in a finite element analysis of the HAZ, and 2) perform a stress relaxation test under various strain conditions to evaluate the susceptibility of stress relaxation cracking. This study was also purposed to quantitatively compare the properties of 347H to those of Super 304H, which is known to have better resistance to stress relaxation cracking.

Experimental Procedures

The dedicated software SYSWELD by ESI was employed for the welding analysis. The tube, including the HAZ, was modeled using 33,520 three-dimensional elements. Goldak's double-ellipsoidal model was applied for the heat source analysis. The variables associated with the shape of the heat source and the energy distribution ratio, which were set by considering the angle and the advancing method of the weld-

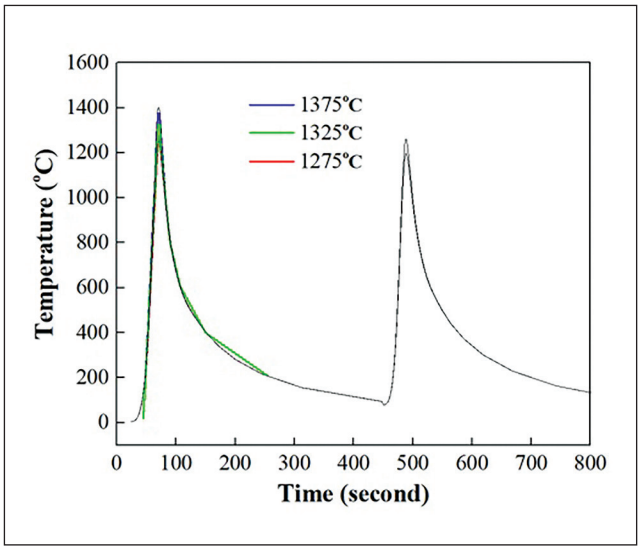

Fig. 2 — Temperature profile observed during simulation of the HAZ.

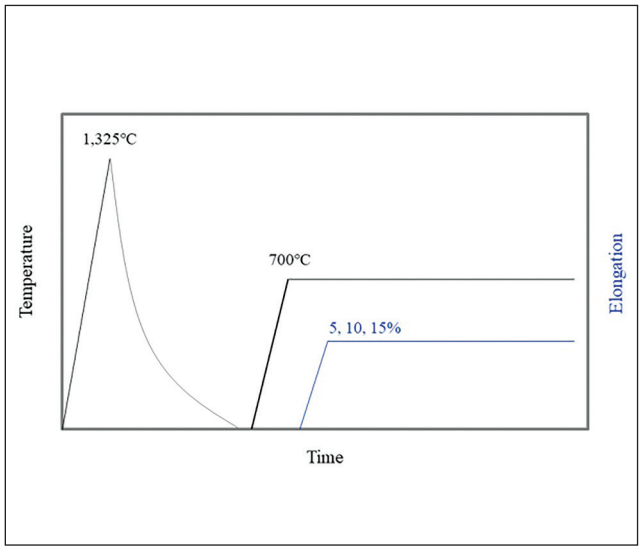

Fig. 3 — Stress relaxation test scheme for 5, 10, and 15% strain conditions.

ing torch, were optimized based on the temperature records from the thermocouple and the bead width. The ambient temperature was maintained at 20°C (68°F) for up to 300 min, and the heat exchange coefficient for free air cooling was used as a surface boundary condition. Thermal analyses were derived from the previous results of the welding specimen production and finite element analysis (Ref. 16). The welding was performed in two passes according to the welding procedure specification of serviced boiler tubes. The temperature profile in the HAZ during welding was determined.

Table 1 presents the chemical compositions of the 347H and Super 304H boiler tubes used in the study. The tubes had diameters of 44.5 and 42.2 mm (1.75 and 1.66 in.), respectively, and a thickness of 7.5 mm (0.29 in.). The test specimen was removed from the boiler tubes and designed in a round bar shape with a diameter of 6 mm (0.24 in.) and a length of 116.5 mm (4.59 in.) — Fig. 1A. After electric discharging machining, the surface of the test specimen was ground and polished. The HAZ simulation and stress relaxation test, which were purposed for the evaluation of the cracking characteristics, were performed using a Gleeble 3800 thermomechanical simulator. The Gleeble system employs a resistance heating method that allows the current to flow directly into the specimen and increase the temperature at a rate of 10,000°C/s (18,000°F/s). Its built-in water-cooling jaw also enables rapid cooling. The specimen was clamped between pocket jaws to prevent it from slipping during straining and holding at test temperature — Fig. 1B.

Thermal cycles with peak temperatures of 1375°, 1325°, or 1275°C (2507°, 2417°, or 2327°F) determined from the SYSWELD analysis were selected to simulate the HAZ using the Gleeble thermomechanical simulator — Fig. 2. It should be noted that the heating and cooling rates applied were consistent with the results of the SYSWELD analysis. No stress was applied to the specimens during the expansion or contraction resulting from the rapid temperature changes. Additionally, an R-type thermocouple placed in the center of each specimen was used to control the thermal cycles in the Gleeble.

To quantitatively evaluate the cracking characteristics in the HAZ, stress relaxation testing was performed by applying the temperature and strain conditions illustrated in Fig. 3 to both types of alloys. First, to simulate the actual HAZ conditions as a result of the microstructural analysis, the temperature was increased to 1325°C and then cooled according to the corresponding HAZ thermal history that was previously obtained. Then, to simulate the thermal stress-induced deformation associated with the welding condition, the specimen was elongated by 5, 10, or 15% at a rate of 0.01 mm/s (0.0004 in./s). The specimen was maintained at the elongated state for a period of 70 h at 700°C (1292°F). For simplicity, the test temperature was fixed at 700°C instead of changing from more than 1200°C (2192°F) to room temperature during welding, and a temperature higher than the service temperature of around 600°C was selected to provide the precipitation effect in a limited time. During this time, the stress change and time to rupture were also monitored and recorded. The temperature was increased from 20° to 700°C at 6°C/s (43°F/s), and the temperature was maintained for 30 s before straining the specimen. A K-type thermocouple was spot welded to the center of each specimen, and a linear variable displacement transducer-type strain gauge was used to measure the elongation at a gauge length of 14 mm (0.55 in.). The stress relaxation test also entailed applying the same 5, 10, and 15% strain conditions to the base metal and HAZ to simulate curved tubes.

After simulating the conditions of the HAZ and performing the stress relaxation test, the cross section of each specimen was ground and polished to enable microstructure analysis. Etching was performed by mixing nitric acid, hydrochloric acid, and pure water at a ratio of 1:2:3. The specimen was then observed at 200 and 500× magnification under an optical microscope. The changes in microstructure relative to the distance from the weld interface in the HAZ were evaluated by applying a scanning electron microscope (SEM; JEOL

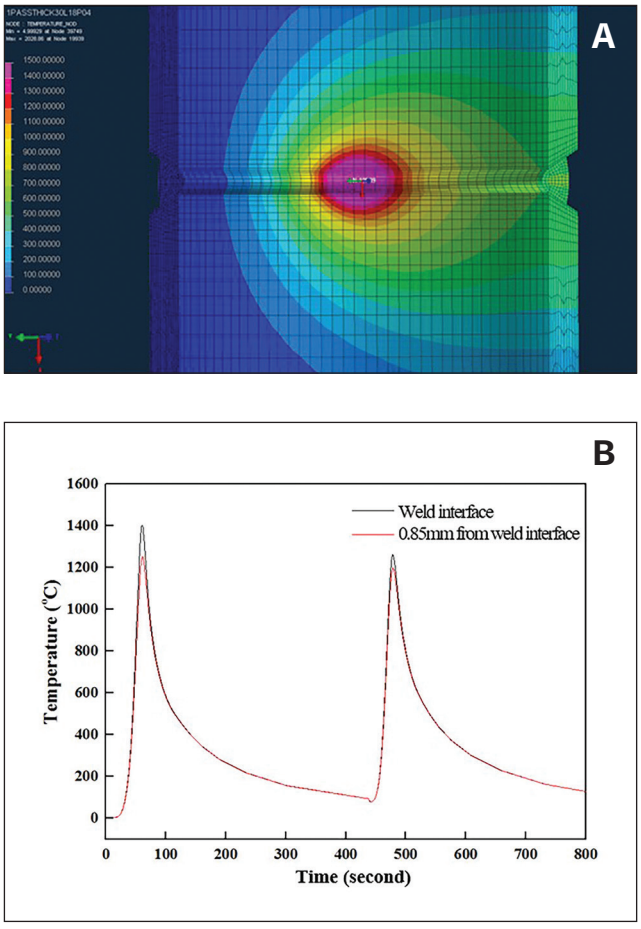

Fig. 4 — Thermal analysis results for the 347H welded joint: A — Heat source and temperature distribution during the first pass; B — temperature profile at the weld interface and in the HAZ.

JSM-7001F). The chemical composition of the precipitates and distribution of the crystal orientations were analyzed by applying energy-dispersive x-ray spectroscopy and electron backscatter diffraction (EBSD). To determine the hardness distribution, an automatic Vickers hardness testing machine (Qness Q10A+) was used to measure the hardness of the HAZ and base metal under the interval conditions of 0.2-mm (0.008-in.) and 200-g (0.44-lb) loading.

Results

HAZ Simulation

Thermal analysis results for the welded joint are shown in Fig. 4. Figure 4A shows the temperature distribution according to the movement of the heat source during the first pass. Figure 4B shows the temperature at the weld interface and in the HAZ (i.e., 0.85 mm [0.03 in.] away) as a function of time during the welding process. The results of the analysis revealed that during the first pass, the temperature increased to approximately 1400°C at the weld interface and approximately 1250°C at a distance of 0.85 mm. The temperatures at both locations subsequently decreased. During the second pass, the temperature increased to more than 1000°C (1832°F) at both locations. Additionally, more than 15% plastic strain was concentrated in the HAZ after the second pass, while there was less than 2% plastic strain after the first pass (Ref. 16). Accordingly, the three temperature conditions of 1275°, 1325°, and 1375°C were selected to simulate several locations with the HAZ.

After simulating the HAZ under three different temperature conditions (Fig. 2), cross sections of the specimen's microstructure were observed under an optical microscope. In the case of the 347H base metal (Fig. 5A), 50~100 µm grains were distributed, with coarse precipitates forming a clustered band along the direction of the tube length. Other fine precipitates were also observed to be distributed in the grains and at grain boundaries. As shown in Fig. 5B, when the HAZ was simulated under the 1275°C condition, no significant difference was observed in terms of grain size or precipitate density. Under the 1325°C condition, the grain size increased to 200 µm and the density of the precipitates was substantially reduced (Fig. 5C). When the HAZ was simulated under the 1375°C condition, incipient melting occurred at the grain boundaries, cracks formed because of the expansion and contraction, and ferrite and eutectic structures formed in some areas (Fig. 5D). The Super 304H microstructure was observed after applying the same method and conditions for HAZ simulation. In the case of the Super 304H base metal (Fig. 5E), the grain size ranged from 20 to 40 µm, which was smaller than that observed during analysis of the 347H microstructure. The precipitates were also relatively smaller in size and high in density. HAZ simulation under the 1275°C condition yielded a grain size range of 40 to 80 µm. The grain size tended to be larger than what was observed to make up the base metal — Fig. 5F. Furthermore, as shown in Fig. 5G, the size of some grains reached 200 µm under the 1325°C condition. Lastly, under the 1375°C condition, incipient melting and cracking occurred at the grain boundaries — Fig. 5H.

The microstructure most similar to that observed under the actual HAZ in a previous study (Ref. 16) seems to have been produced under the 1325°C condition in the cases of both steel types. Figure 6 shows hardness measurement results for the 1325°C condition of both steel types. Figure 6A presents the results for the 347H simulated HAZ specimen. When the hardness distribution was examined using 0.2-mm intervals, the simulated HAZ was clearly distinct from the unaffected zone. The average hardness of the unaffected zone was approximately 180 HV, whereas that of the HAZ was 154 HV, indicating that the heat treatment significantly reduced the hardness in the HAZ. This difference may be related to the significant decrease in the density of the precipitates in the HAZ as well as the increase in the average grain size. During welding, the temperature of the HAZ gradually approached the melting temperature. During this time, a significant amount of the niobium carbide was dissolved into the HAZ. Additionally, the dissolved carbon was partially reprecipitated during the rapid cooling process, thereby nullifying the stabilizing effect. As shown in Fig. 6B, the hardness of the unaffected zone of the Super 304H was 186 HV, which was similar to that of 347H. However, the hardness of the Super 304H HAZ was 172 HV, which did not correspond to

a significant reduction. Furthermore, this hardness value was higher than that measured in the 347H HAZ. It should also be noted that although the extent of the Super 304H HAZ grain size increase was comparable to that of the 347H HAZ, the hardness did not significantly decrease.

To quantitatively evaluate the difference in hardness reduction in the HAZ according to steel type, the distribution of precipitates in the HAZ and the unaffected zone was compared by using a SEM. Figures 7A and B show the precipitate distribution in the unaffected zone and the 347H HAZ, respectively. As shown in Fig. 7A, in the unaffected zone, coarse precipitates approximately 1 μm in size were distributed along the grain boundaries, and fine precipitates were distributed within the grains. Most intragranular precipitates in the HAZ (Fig. 7B) were observed to have dissolved and disappeared, leaving only some fine precipitates along the grain boundaries. In the case of the Super 304H unaffected zone, more fine precipitates less than 1 μm in size were uniformly distributed within grains and along grain boundaries. This was not observed in the case of 347H — Fig. 7C. Further analysis of the Super 304H HAZ (Fig. 7D) revealed that some precipitates had dissolved and disappeared, and fine precipitates were present in the grains. Nevertheless, as compared to the 347H HAZ, a relatively large number of precipitates remained. The degree of precipitate dissolution before and after welding simulation could be compared by using image analysis — Fig. 7. The area fractions of the precipitate in the 347H base metal and HAZ were 0.7 and 0.2%, respectively. In addition, the Super 304H base metal and HAZ included precipitates of 1.3 and 0.8% area fraction.

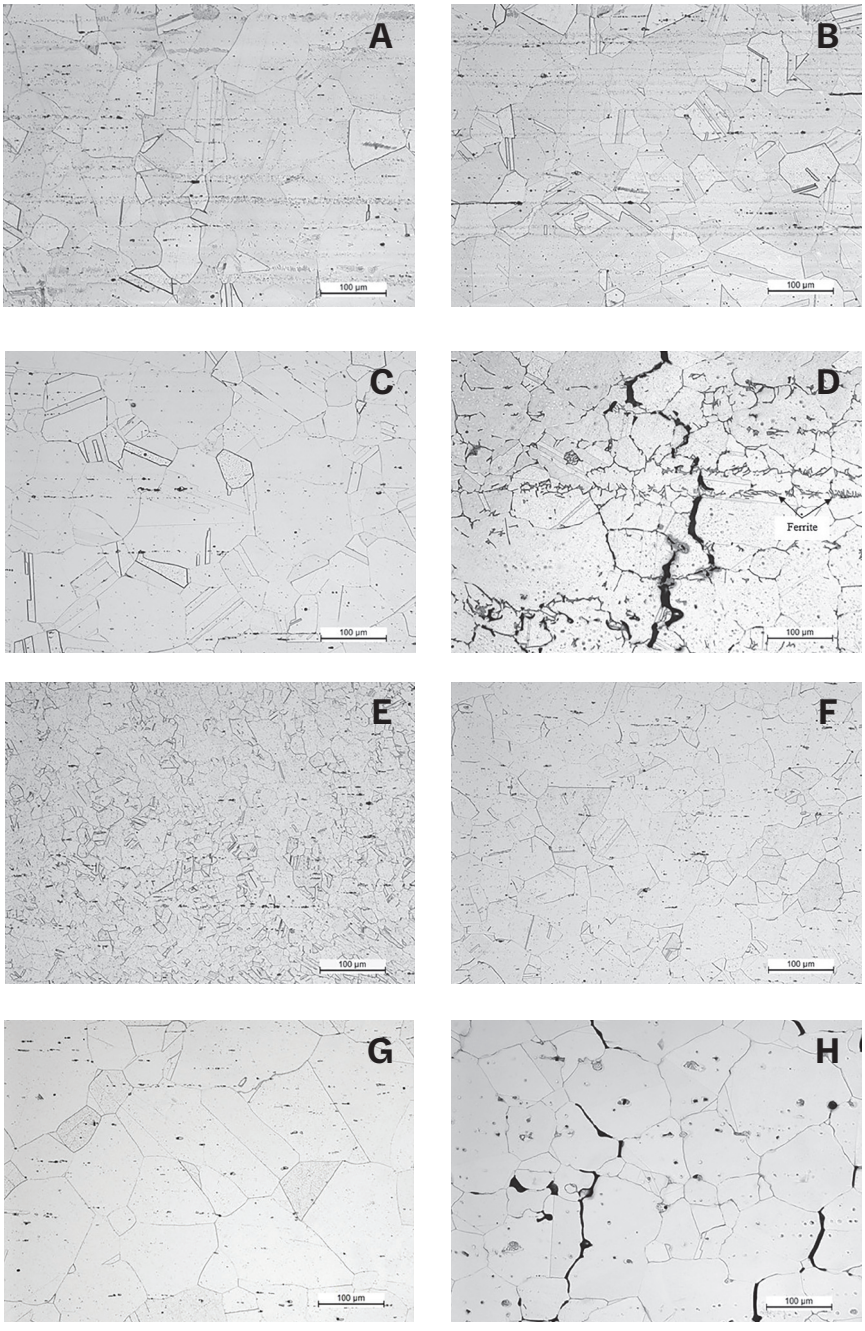

Fig. 5 — Optical images of the base metal and simulated HAZ cross sections: A–D — 347H base metal at 1275°, 1325°, and 1375°C conditions, respectively; E–H — Super 304H base metal at 1275°, 1325°, and 1375°C conditions, respectively.

Stress Relaxation Test

Table 2 shows the stress relaxation test results for each strain condition for the 347H base metal and HAZ. Under the 5% strain condition for the 347H base metal, fracturing occurred 31.9 h after the start of the test. Increasing the strain to 10 and 15% significantly reduced the fracture time to 2.2 and 1.4 h, respectively. The HAZ results revealed a shorter rupture life compared to that of its 347H base metal counterpart under all strain conditions. More specifically, rupture occurred at 26.8, 1.3, and 0.9 h under the conditions of 5, 10, and 15% strain, respectively. Increasing the strain to 10% coincided with a sharp decrease in the time to rupture.

Table 2 also provides the results for the time to rupture and stress relaxation percentage, which is defined as the percentage of stress remaining at rupture. Under the 5% strain condition, which coincided with a relatively long rupture life, the stress relaxation percentage was more than 50%. Conversely, under the 10 and 15% strain conditions, which coincided with significantly shorter rupture lives, the

Table 2 — Stress Relaxation Results for the Base Metal and Its Simulated HAZ

347H		Rupture Time (h)	Initial Stress (MPa)	Fracture Stress (MPa)	Stress Relaxation (%)
	5%	31.8	294	139	53
Base metal	10%	2.2	323	215	33
	15%	1.4	338	227	33
	5%	26.7	281	139	51
HAZ	10%	1.3	324	222	31
	15%	0.9	337	220	35
Super 304H		**Rupture Time (h)**	**Initial Stress (MPa)**	**Final Stress (MPa)**	**Stress Relaxation (%)**
Base metal	15%	Nonfailed	349	174	49
HAZ	15%	Nonfailed	352	166	47

stress relaxation percentage was relatively low (i.e., ranging between 30 and 40%). The same stress relaxation test was applied to Super 304H. The test results are shown in Fig. 8 along with the 347H results. In the case of 347H, the rupture occurred within 32 h regardless of the strain condition. The rupture was also preceded by rapid stress reduction. In the case of Super 304H, rupture did not occur within the 70-h observation limit even under the 15% strain condition. This was true for both the base metal and HAZ. Initially, the stress rapidly decreased. However, Super 304H tended to maintain a higher stress level than 347H over time.

First, after the stress relaxation testing was completed, a cross section of the microstructure of each specimen was observed. Intergranular cracks were observed under all strain conditions in the cases of the 347H base metal and simulated 347H HAZ, respectively — Figs. 9A, B. Additionally, a large number of cracks were observed to have formed perpendicular to the direction of stress and distributed near the fractured surface. In the case of the base metal (Fig. 9A), the cracks were only concentrated near the fractured surface. However, analysis of the HAZ microstructure (Fig. 9B) revealed the existence of intergranular cracks throughout the entire simulated HAZ. The microstructure of the Super 304H, which did not rupture during the stress relaxation test, was not observed to have intergranular cracks like those observed in the 347H microstructure. However, microcracks or pores that ran perpendicular to the direction of stress were identified in and around the precipitates — Figs. 9C, D.

Second, hardness analysis was performed after the stress relaxation test. Figures 10A–F show the hardness distribution results for the 347H specimen. The initial hardness was measured to be approximately 180 HV. However, the hardness values of the base metal and HAZ significantly increased in response to being subjected to the stress relaxation test. As shown in Fig. 10A, under the 5% strain condition, the average hardness of the 347H base metal was 230 HV at the center of the specimen where the fracture occurred. This value increased to 249 and 250 HV in response to an increase in the strain by 10 and 15%, respectively — Figs. 10B, C. As shown in Figs. 10E and F, under the 10 and 15% strain conditions, a

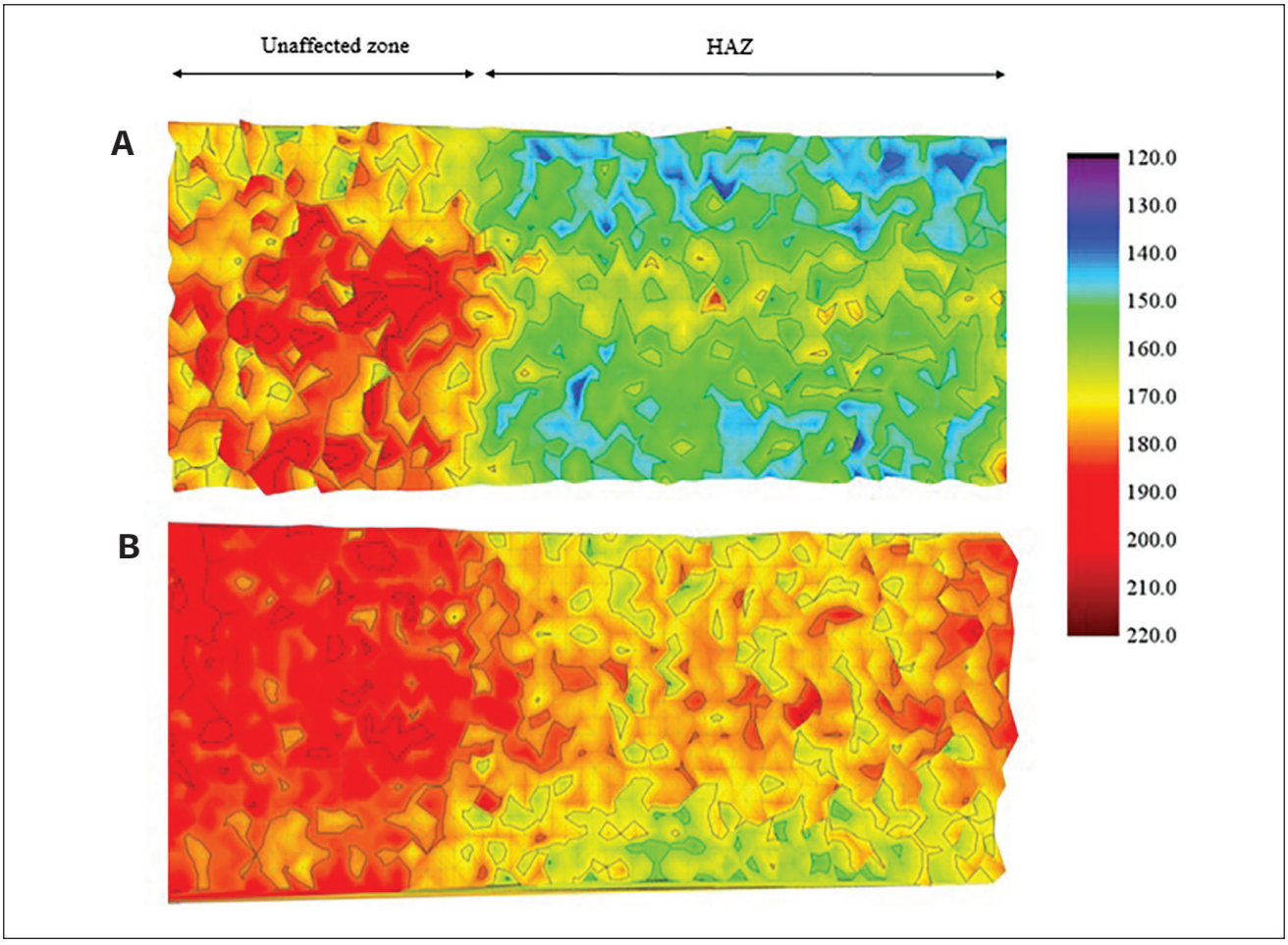

Fig. 6 — Microhardness distribution after the HAZ simulation at 1325°C: A — 347H; B — Super 304H.

clearly distinguished boundary was observed between the HAZ and the unaffected zone of the specimen.

Furthermore, the increase in hardness was mainly limited to the HAZ. The average HAZ hardness values were 250 HV (10%) and 256 HV (15%), which were higher than that of its base metal counterpart. Under the 5% strain condition, as displayed in Fig. 10D, the difference in hardness between the HAZ and the unaffected zone of the ruptured specimen was not large. However, under the 10 and 15% strain conditions, the hardness of the cracked HAZ was approximately 20 HV higher than that of the unaffected zone. Alternatively, the results of the Super 304H base metal under the 15% strain condition (Fig. 10G) revealed that the large strain did not significantly affect the initial uniformity of the hardness distribution (i.e., the average hardness was 250 HV). This was not true for 347H. Additionally, although the hardness of Super 304H was higher in the simulated HAZ under the 15% strain condition (Fig. 10H), the difference between its HAZ and unaffected zone hardness was not as large as that of 347H. The hardness of the HAZ was 263 HV, and the hardness of the unaffected zone was 251 HV. According to the results, the strain was uniformly distributed throughout the 347H, and the specimen could uniformly distribute the applied strain when it was less than or equal to 5%. However, applying a 10 or 15% strain resulted in strain concentration at the center of the specimen, which significantly increased the hardness in that area.

Lastly, EBSD analysis was performed to support the microstructural analysis results for the crack formation region, which corresponds to the region in which the strain was concentrated, and the hardness was higher. Measurements were performed at intervals of 0.5 µm. Figure 11 provides the results of the EBSD analysis. The legend shows how the results were classified according to misorientation angle and type of crystal structure (i.e., face-centered cubic [FCC] or body-centered cubic [BCC] structure). In general, the grain and twin boundaries had large misorientation angles relative to neighboring positions, and the angles between neighboring measurement positions were the same for the same grain. The poststress relaxation test analysis of a cross section of the fractured surface of the 347H specimen revealed crack initiation, propagation, and intersection along the grain boundaries under all conditions. This eventually led to the rupture of the specimen.

As can be ascertained from Figs. 11A and B, under the 5% strain condition, misorientation angles of at least 1 deg tended to exist near the grain boundaries regardless of the treatment condition. The area with the most significant change in crystal orientation was found to have cracks that tended to propagate in the horizontal direction, which was

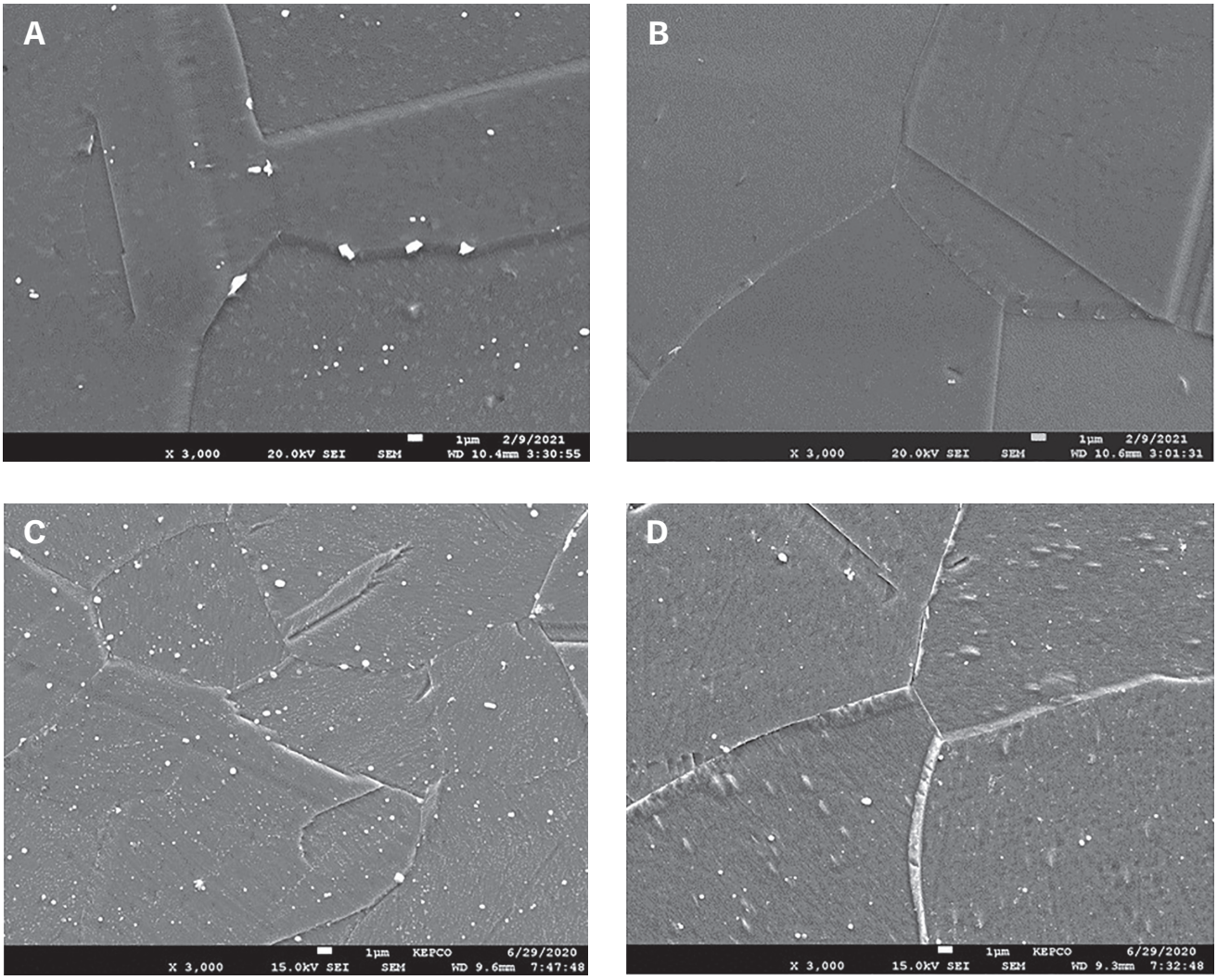

Fig. 7 — SEM micrographs: A — 347H base metal; B — simulated 347H HAZ; C — Super 304H base metal; D — simulated Super 304H HAZ.

perpendicular to the direction of stress observed during the stress relaxation test. In addition, as can be seen in Fig. 11B, there was more strain concentration along the grain boundaries in the HAZ than in the base metal — Fig. 11A. As can be seen in Figs. 11C and D, which show the 15% strain condition results, the size of the area containing misorientation angles of at least 1 deg was significantly higher than that observed for the 5% strain condition. As the strain increased from 5 to 15%, the degree of plastic deformation near the fractured surface increased and was found to be higher near the grain boundaries.

Discussion

Cracking Susceptibility

In a previous study on stress relaxation cracking occurring in the HAZ of welded 347 stainless steel, temperatures ranging between 1150° (2102°) and 1300°C (2372°F) were applied in a hot ductility test by using Gleeble to simulate the HAZ (Ref. 17). This method yielded results that can be used to determine the temperature at which melting begins to occur at grain boundaries as well as the temperature at which there is a sudden decrease in elongation. This can be determined by applying the tensile strain at a rapid rate during heating and cooling and measuring the extent of the reduction of area after rupture. However, the hot ductility test is a method for evaluating the hot cracking susceptibility, not the stress relaxation cracking susceptibility (Refs. 18, 19). Studies that entailed the application of hot ductility tests to various types of austenitic stainless steels reported significant differences in the temperature range at which partial melting occurred. These studies also reported that the temperature range was dependent on the chemical composition, even among the specimens of the same 347 steel grade (Refs. 20, 21).

Thus, this study was conducted as an attempt to reproduce the HAZ conditions based on the results of finite element analysis for welded specimens. The results of finite element and microstructural analyses indicated that applying a simulation heating temperature of 1325°C created conditions that

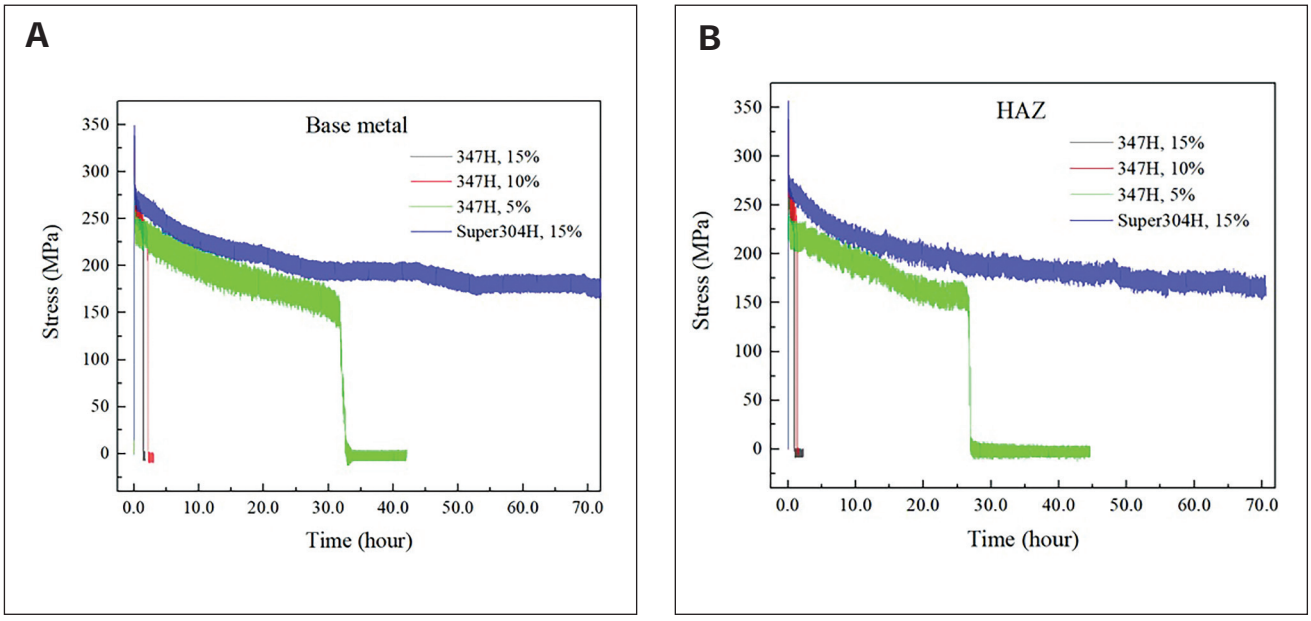

Fig. 8 — Stress relaxation curves: A — Base metal; B — HAZ.

were most similar to those associated with an actual HAZ. The stress relaxation test results for the 347H base metal revealed that the rupture life tended to decrease with the increase in applied strain from 5 to 15%. When the strain was increased to 10%, the rupture life sharply decreased. Furthermore, the results of the HAZ simulation revealed that the rupture life tended to be shorter than that of its base metal counterpart. In the case of Super 304H, neither the base metal nor the HAZ ruptured within the 70-h observation period.

In general, stress relaxation refers to a phenomenon in which the stress decreases over time when the strain is kept constant under the condition of a constant temperature. The reduction in stress occurs during the transition from elastic strain to plastic strain (Ref. 22). Thus, the crack initiation, crack growth, and rupture life may have been affected by the area and degree of plastic strain concentration during the stress relaxation test. As a result, it was deemed necessary to analyze these relationships by comparing the microstructural differences between the HAZ and base metal as well as between stainless steel types.

Kant and DuPont performed a stress relaxation test after simulating the HAZ in nickel alloys and stainless steels (Ref. 23). They determined the relative crack susceptibility based on a four-category classification system for crack shapes on the fractured surface. The first category consisted of only intergranular cracks that occurred without grain deformation. The second category was comprised of intergranular cracks that were accompanied by grain deformation. The third category included a mixture of intergranular and transgranular cracks. Lastly, the fourth category was made up of ductile fractures that occurred in the presence of pore formation. According to this classification system, the microstructure of the 347H used in this study indicated consistency with the first category, which corresponds to the highest cracking susceptibility — Figs. 9A, B. Because Super 304H did not rupture and was observed to have limited pore formation (Figs. 9C, D), it was thought to have low cracking susceptibility. In the case of 347H, cracks propagated and intersected along the grain boundaries, leading to sudden rupture. Thus, as can be seen in the stress relaxation curve presented in Fig. 8, a discontinuous and abrupt change in the slope occurred at the end of the test. A comparison of the aforementioned results for the rupture life and microstructure revealed that Super 304H has relatively superior stress relaxation characteristics and cracking resistance.

Strain-Induced Precipitation Hardening

Strain-induced precipitation hardening occurs in a region with a high hardness value due to the concentration of deformation, which consequently leads to high cracking susceptibility. 347H was able to maintain a uniform hardness distribution throughout the specimen under the 5% strain condition. However, under the 10 and 15% strain conditions, the hardness significantly increased in the center of the specimen (i.e., the prominent crack formation and propagation region). The results of simulating the HAZ also revealed the existence of a boundary between the HAZ and unaffected zone. Additionally, there was a relatively large difference in hardness between the two areas. However, the Super 304H alloy was able to maintain its uniform hardness distribution under the 15% strain condition. It can be thought that the strain concentration of 347H consequently promoted crack initiation. Super 304H is considered to have low cracking susceptibility because it was demonstrated to prevent strain concentration even under the conditions with relatively large strains of up to 15%.

In addition, the HAZ simulation results indicated that the difference between 347H and Super 304H HAZ hardness may be related to the dissolution of the initial precipitates. Because 347H is an alloy steel to which niobium has been added as a stabilizing element to improve intergranular

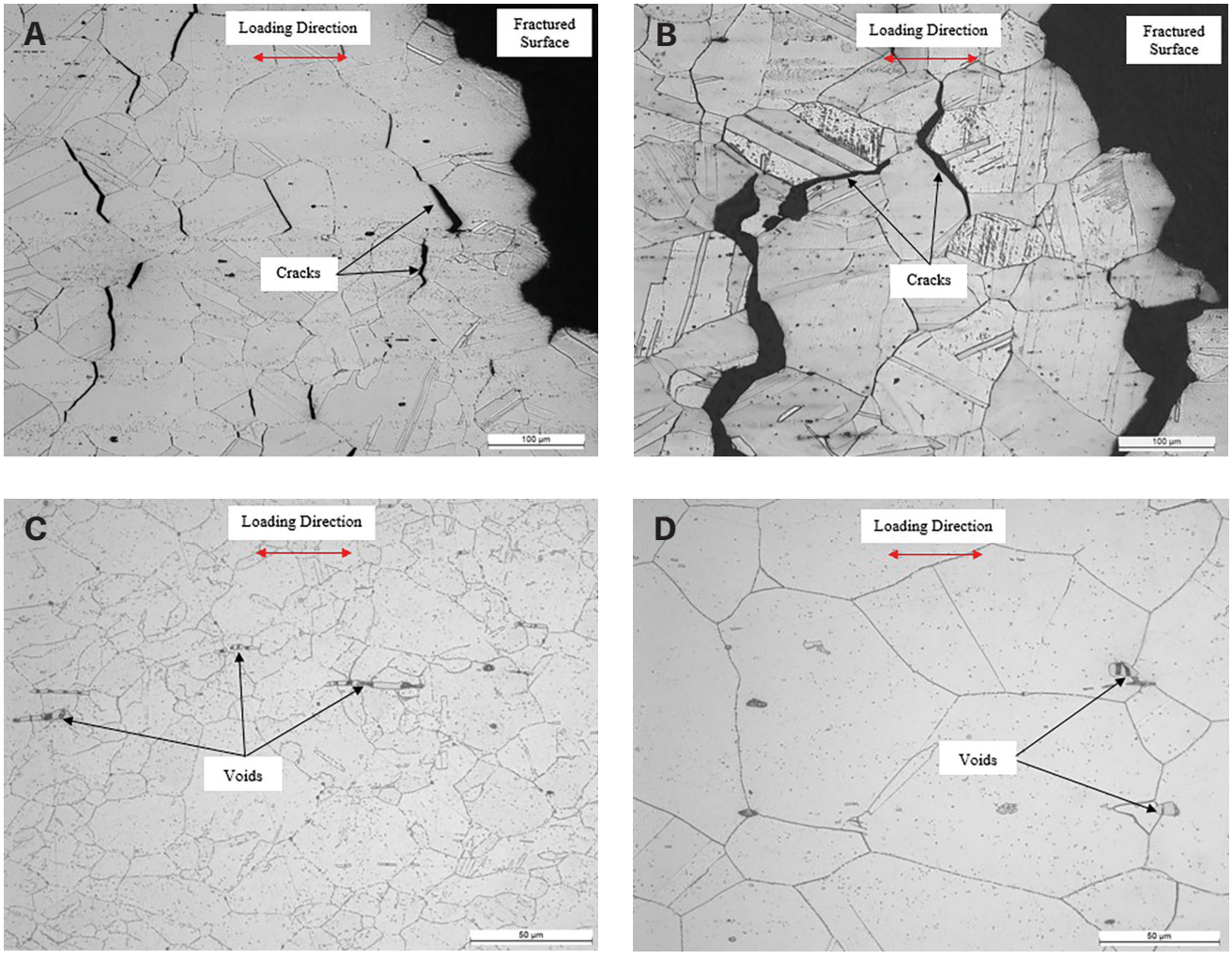

Fig. 9 — Optical images showing the poststress relaxation test cross sections of the following: A — 347H base metal; B — simulated 347H HAZ; C — Super304H base metal; D — simulated Super304H HAZ.

corrosion, niobium carbide, instead of chromium carbide, tended to precipitate. In the case of Super 304H, copper and nitrogen have been added. This allowed the heat treatment to refine the grains. Furthermore, Super 304H tends to be strengthened by the copper phase and niobium nitride, which constitute the coherent precipitates (Refs. 24–27). Popov (Ref. 28) compared the dissolution of carbides and nitrides under various solution heat treatment temperature conditions. He reported the occurrence of less nitride dissolution than carbide dissolution at the same temperature. These findings are consistent with the results obtained in this study, which indicate that the difference in hardness between the Super 304H unaffected zone and HAZ was smaller than that of the 347H because the addition of nitrogen resulted in less precipitate dissolution in the HAZ.

Strain-induced precipitation hardening is caused by deformation during welding and bending processes. Upon aging in operation, the hardness of both the base metal and HAZ regions increase due to precipitation, but within the grains, very fine carbides precipitate due to the preexisting dislocation substructure. The process of relaxation cracking is due to rapid precipitation of very fine matrix carbides on dislocation knots, which block dislocation motion. At temperatures between 550° (1022°) and 750°C (1382°F), the fine precipitates coarsen slowly, allowing the dislocations to stay blocked. Thus, the matrix cannot deform, and the stresses are reduced by creep deformation that is concentrated in the grain boundary region. This causes intergranular failure (Ref. 29).

As a result, when the 347H is exposed to high temperatures, a large number of fine precipitates form in the grains. Alternatively, coarse precipitates form along the grain boundaries because of the high diffusion rate. The formation of a precipitation-denuded zone near grain boundaries leads to strain concentration along grain boundaries and crack formation. Under all of the testing conditions corresponding to the results shown in Figs. 11A–D, the strain became concentrated along the grain boundaries, which were perpendicular to the direction of stress. The effects of strain-induced precipitation hardening could be identified by evaluating the increase in areas with a misorientation angle of at least 1 deg as a function of the increase in strain.

Lee et al. analyzed the case of stress relaxation cracking-related damage in the 347H HAZ of a power plant boiler

(Ref. 16). The dissolution of niobium carbide, which lost its stabilizing effect during grain coarsening, was observed in the HAZ immediately after it was welded. Additionally, the hardness of the inner surface of the tube was found to have significantly increased. This is because solidification of the weld interface introduced thermal stress that resulted in deformation. After 4000 h of operation, the EBSD analysis of the HAZ revealed the existence of damage related to stress relaxation cracking, which was caused by strain-induced precipitation hardening. Specifically, it was observed that the strain and crack propagation was concentrated near the grain boundary.

Figures 11E and F show the effects of applying 15% strain to the base metal and HAZ, respectively, on the crystal orientation of Super 304H. It can be seen that neither cracks nor rupture occurred even after it was subjected to the stress relaxation test, which merely induced the formation of fine pores that were primarily concentrated in and around the precipitates. Additionally, Fig. 11E shows that the application of the 15% strain condition to the base metal specimen yielded grains that were smaller in size than those of the 347H specimen. It can also be seen that the misorientation angle of at least 1 deg was more evenly distributed than that of 347H, which was concentrated at the grain boundaries. In the case of the HAZ simulation, under the 15% strain condition (Fig. 11F), the grain size was significantly larger than that of its base metal counterpart and was similar to that of the 347H specimen. Additionally, the area with a large local misorientation angle was smaller than that observed in the case of 347H — Fig. 11E. It was also not concentrated along the grain boundaries.

The microstructure of austenitic stainless steels such as 347H and Super 304H can be sensitive to manufacturing processes consisting of softening heat treatment, cold drawing, and final solution treatment. As can be seen from their microstructures, 347H and Super 304H differ in the manufacturing process. After cold drawing, 347H is given a high-temperature solution treatment, which causes recrystallization and grain growth. The final solution treatment is also conducted at a high temperature to dissolve the niobium carbide and put the niobium into a solution that precipitates as niobium carbide during operation. However, Super 304H requires a softening treatment of at least 50°C above the final solution temperature. This is intended to dissolve the coarser niobium carbides while preserving sufficient fine niobium nitrides to help pin grain boundaries and limit grain growth during the final solution treatment (Ref. 30). In a study on stress relaxation cracking in the HAZ of 347 stainless steel, quantitative evaluation of various factors revealed that the grain size, amount of niobium carbide, and heating and cooling rates were the major factors affecting the rupture life (Ref. 17). A smaller grain size and a higher amount of precipitate resulted in a longer time to failure, which indicates lower cracking susceptibility.

Unlike 347H, Super 304H is able to maintain the stabilizing effect provided by the higher amount of niobium nitride or carbonitride. This is because the nitrogen in the alloy steel served to mitigate the dissolution of precipitates. Thus, the excellent cracking characteristics of Super 304H can be attributed to its ability to maintain a relatively small grain

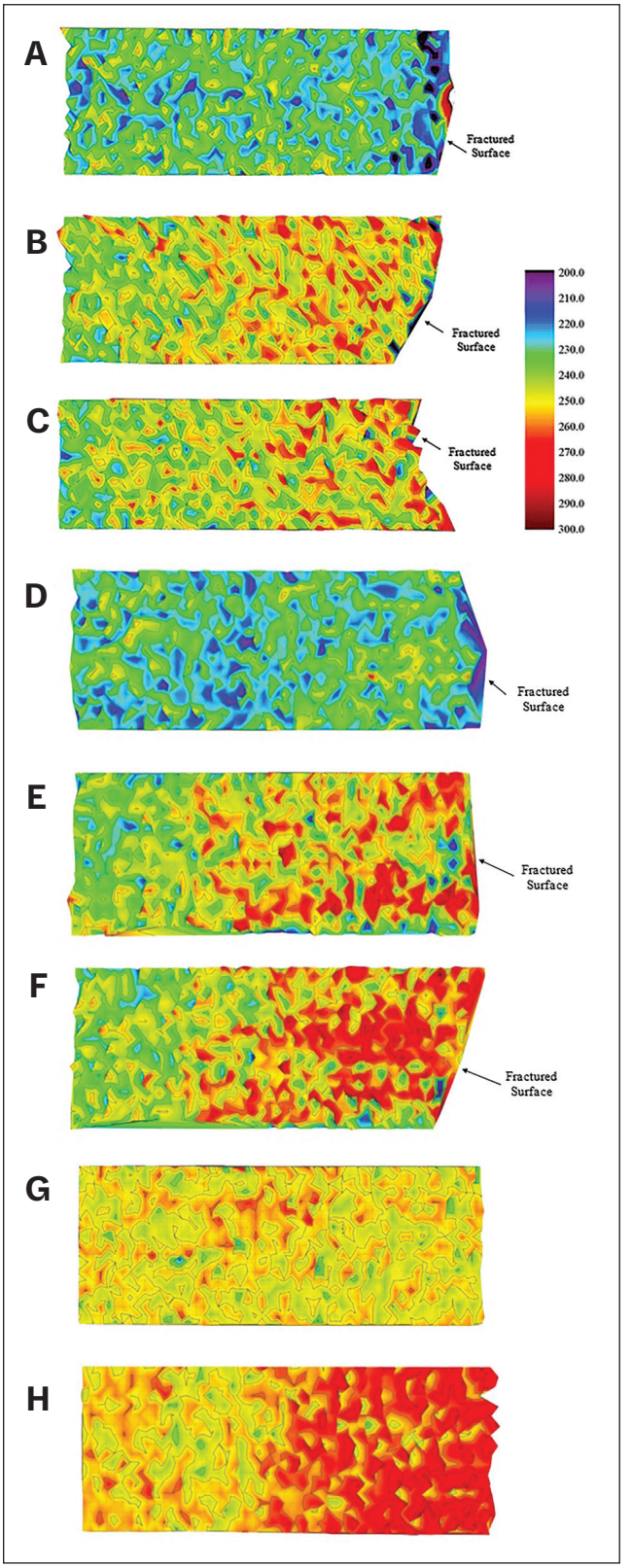

Fig. 10 — Poststress relaxation test microhardness distribution: Elongation of the 347H base metal at 5 (A), 10 (B), and 15% (C); elongation of the simulated 347H HAZ at 5 (D), 10 (E), and 15% (F); elongation of the Super 304H base metal at 15% (G); and elongation of the simulated Super304H HAZ at 15% (H).

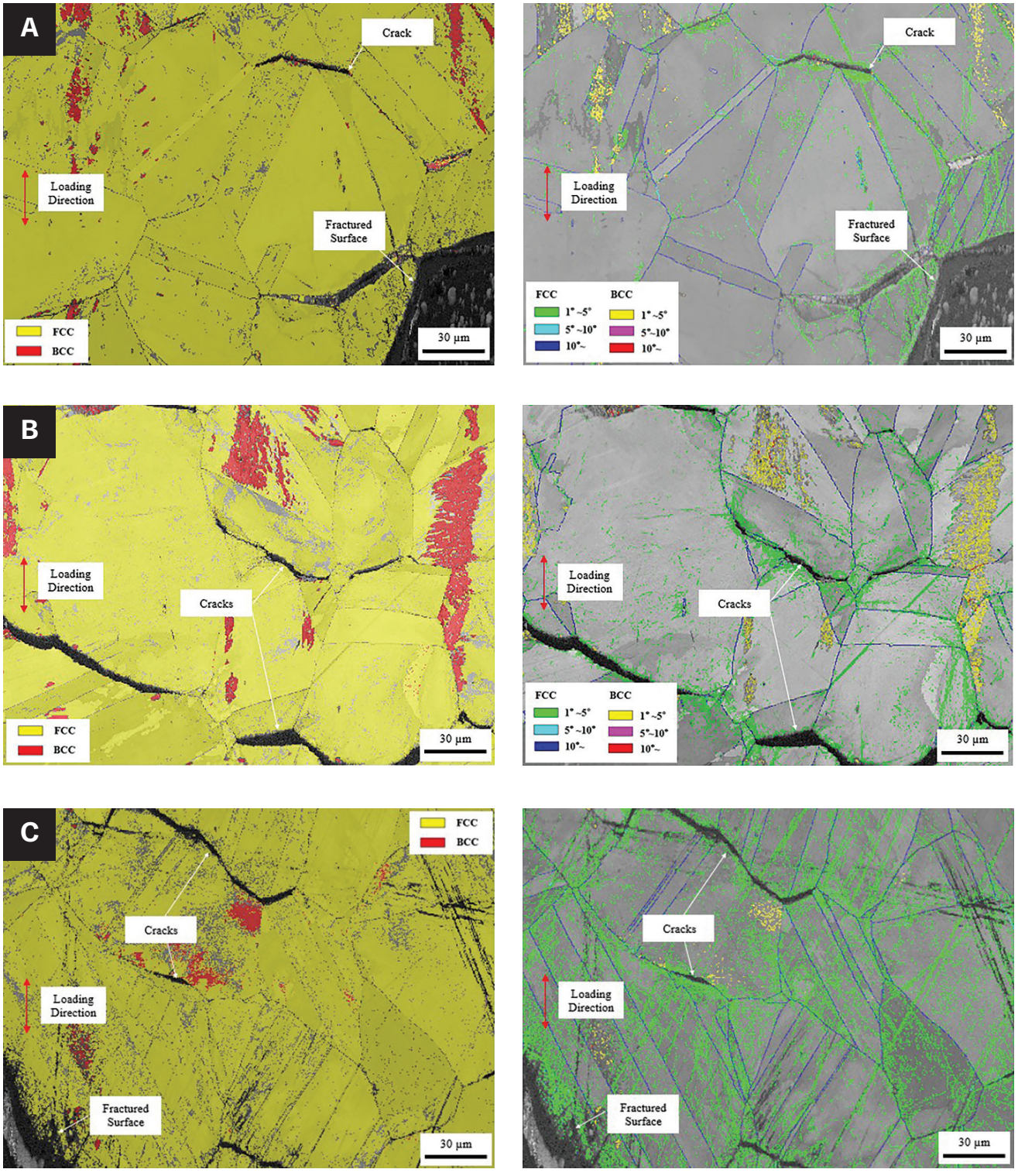

size and large grain boundary areas, which prevented the strain concentration.

Strain-Induced Martensite

Strain-induced martensites with a BCC structure were also observed under all conditions. However, their size varied. The BCC structures were relatively wider in the case of the HAZ simulation (Figs. 11B and D) than in the case of the base metal specimen (Figs. 11A and C) and occupied up to 15%. Austenitic stainless steels such as 347H form an austenite phase with a metastable FCC structure in the presence of chromium and nickel. The austenite phase in metastable stainless steel is susceptible to strain-induced martensite transformation. Hence, the austenite might have partially transformed to martensite. Okayasu et al. examined strain-induced martensite formation by applying tensile testing to 304 stainless steel. They reported that the strain-induced

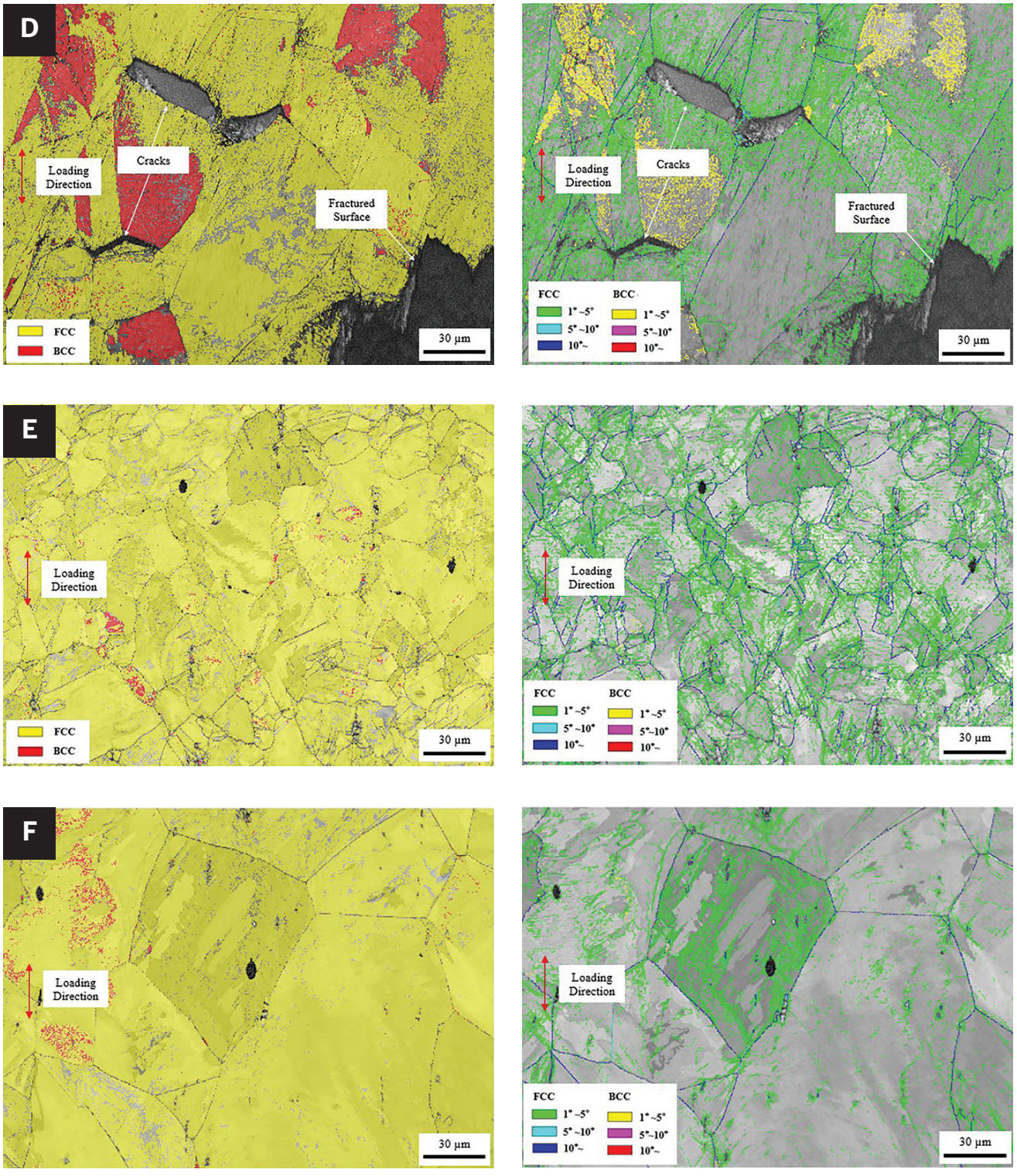

Fig. 11 — Results of the poststress relaxation test EBSD analysis: A — 5% elongation of the 347H base metal; B — 5% elongation of the simulated 347H HAZ; C — 15% elongation of the 347H base metal; D — 15% elongation of the simulated 347H HAZ; E — 15% elongation of the Super 304H base metal; F — 15% elongation of the simulated Super 304H HAZ.

martensite formed above the yield strength, occupying a considerable area above the tensile strength (Ref. 31). Additionally, Masumura et al. reported the increase in the volume fraction of strain-induced ά-martensite (BCC structure) as a function of thickness reduction by cold rolling for 304 stainless steel containing 0.1C or 0.1N (Ref. 32). The increasing rate of ά-martensite formation for carbon and nitrogen was similar to the thickness reduction of less than 30%. In a previous study that analyzed the case of cracking damage in the HAZ of 347H boiler tubes, the results of EBSD analysis

revealed the existence of an area on the inner surface of the tube, where cracks had occurred, that had BCC crystal structures. Further analysis of the characteristics of this area indicated that strain-induced martensite had formed during the welding process (Ref. 16).

This was taken into consideration in the analysis of the simulated HAZ in this study. The 347H HAZ was found to have a higher hardness and a higher volume fraction of strain-induced martensite. This occurred because the amount of strain applied during the stress relaxation test was concentrated in the HAZ. The strain-induced martensite formed during the straining step but not during the stress relaxation step. As a result, the formation of strain-induced martensite and the increase in area confirmed that deformation is concentrated in the HAZ.

Conclusion

The results of using a thermomechanical simulator (Gleeble 3800) to conduct HAZ simulation, as well as those obtained by performing stress relaxation testing under 5 to 15% strain conditions to evaluate the cracking characteristics of 347H and Super 304H stainless steel boiler tubes, yielded the following results:

1) Under the HAZ simulated condition, the size of the 347H grains increased to up to 200 μm and the amount of the precipitates significantly decreased. In the case of Super 304H, the size of the grains also increased to a size similar to that observed in the 347H microstructure, but relatively few precipitates were found to have dissolved. Additionally, comparison of the hardness of the base metals and their HAZ counterparts revealed that, in the case of Super 304H, the difference in hardness was insignificant, unlike that observed in the case of 347H.

2) The stress relaxation test results for 347H revealed that the rupture life tended to decrease with the increase in applied strain. When the strain was increased to 10%, the rupture life sharply decreased. In the case of Super 304H, neither the base metal nor the HAZ ruptured within the 70-h observation period.

3) Fractured surface analysis of 347H confirmed the formation and propagation of cracks along the grain boundaries in a direction that was perpendicular to the direction of stress. Additionally, the misorientation was concentrated around the grain boundaries. The increasing strain level was found to correspond with the gradual increases in the misoriented area around the grain boundaries. This is the evidence of strain location that was in turn due to matrix strengthening by strain-induced precipitation hardening.

4) The hardness profile of 347H showed a local increase from the 10% strain condition, while Super 304H maintained the uniform hardness distribution up to 15% strain condition. Strain-induced martensite of up to 15% area fraction was observed in the area with locally high hardness. As a result, strain-induced martensite as well as strain hardening and strain-induced precipitation hardening contributed to the higher HAZ hardness in 347H.

Acknowledgment

This work was supported by the Korea Electric Power Corp. under Grant Nos. R19GA04 and R21GH01.

References

1. Ahn, J., Park, J., and Lee, G. 2015. Effect on the stabilizing heat treatment to weld joint for the USC coal boiler tubes. *Journal of Welding and Joining* 33(4): 30–36. DOI: 10.5781/JWJ.2015.33.4.30

2. Park, S. K., Lee, H. J., and Lee, J. H. 2018. Effects of thermal aging induced microstructure evolution on mechanical and corrosion properties of delta-ferrite in austenitic stainless steel weld. *Korean Journal of Metals and Materials* 56(4): 296–303. DOI: 10.3365/KJMM.2018.56.4.296

3. Park, H. 2003. Cracking in welds and its prevention. *Journal of the Korean Welding Society* 21(1): 5–7.

4. van Wortel, H. 2007. Control of relaxation cracking in austenitic high temperature components. *NACE Corrosion Conference and Expo*, Houston, Tex. NACE International.

5. Li, L., and Messler, R. W. 2000. The effects of phosphorus and sulfur on susceptibility to weld hot cracking in austenitic stainless steels. *Welding Journal* 79(6): 138-s to 144-s.

6. ASME *Boiler and Pressure Vessel Code, Section I, Rules for Construction of Power Boilers*. 2017. The American Society of Mechanical Engineers.

7. Shingledecker, J. 2013. *The Advanced Austenitic Stainless Steels Handbook*. Palo Alto, Calif.: Electric Power Research Institute.

8. Lee, H., Kim, H., Park, M., Kim, B., and Lee, J. 2020. Welding process improvement of 347H stainless steel boiler tube for mitigating reheat cracking. *Journal of Welding and Joining* 38(6): 551–562. DOI: 10.5781/JWJ.2020.38.6.5

9. Lippold, J. C. 2014. *Welding Metallurgy and Weldability*. New York: John Wiley & Sons.

10. Pense, A. W., Galda, E. J., and Powell, G. T. 1971. Stress relief cracking in pressure vessel steels. *Welding Journal* 50(8): 374-s to 378-s.

11. Nishimoto, K., Matsunaga, T., Tanaka, T., and Okazaki, T. 1998. Effect of bismuth on reheat cracking susceptibility in Type 308 FCA weld metal. *Welding in the World* 41: 220–235.

12. Tamaki, K., and Suzuki, J. 1983. Reheat cracking test on high strength steels by a modified implant test. *Transactions of the Japan Welding Society* 14(2): 33–38. DOI: 10.2207/qjjws1943.50.1198

13. Younger, R. N., and Baker, R. G. 1960. Heat-affected zone cracking in welded high-temperature austenitic steels. *JISI* 196: 188–194.

14. Nawrocki, J. G., Dupont, J. N., Robino, C. V., Puskar, J. D., and Marder, A. R. 2003. The mechanism of stress-relief cracking in a ferritic alloy steel. *Welding Journal* 82(2): 25-s to 35-s.

15. Norton, S. J., and Lippold, J. C. 2002. Development of a Gleeble-based test for postweld heat treatment cracking susceptibility. *Proceedings of the 6th International Trends in Welding Research Conference*, 15–19. Phoeniz, Ariz.

16. Lee, H., Jung, J., Kim, D., and Yoo, K. 2015. Failure analysis on welded joints of 347H austenitic boiler tubes. *Engineering Failure Analysis* 57: 413–422. DOI: 10.1016/j.engfailanal.2015.08.024

17. Isaratat, P. 2007. An investigation of reheat cracking in the weld heat affected zone of type 347 stainless steel. PhD diss., The Ohio State University.

18. Weiss, B., Grotke, G. E., and Stickler, R. 1970. Physical metallurgy of hot ductility testing. *Welding Journal* 49(10): 471-s to 487-s.

19. Lundin, C. D., Qiao, C. Y. P., Gill, T. P. S., and Goodwin, G. M. 1993. Hot ductility and hot cracking behavior of modified 316 stainless steels designed for high-temperature service. *Welding Journal* 72(5): 189-s to 200-s.

20. Lundin, C. D., Lee, C. H., Menon, R., and Osorio, V. 1988. Weldability evaluations of modified 316 and 347 austenitic stainless steels: Part 1 — Preliminary results. *Welding Journal* 67(2): 35-s to 46-s.

21. Lee, Y. H., Lee, C. H., and Lundin, C. D. 1988. Hot ductility and hot cracking susceptibility of Type 303 austenitic stainless steel (1) — Hot ductility behavior. *Journal of the Korean Welding and Joining Society* 6(1): 35–45.

22. Manjoine, M. J., and Voorhees, H. R. 1982. Compilation of Stress-Relaxation Data for Engineering Alloys. Philadelphia: ASTM Data Series Publication DS60.

23. Kant, R., and DuPont, J. 2019. Stress relief cracking susceptibility in high-temperature alloys. *Welding Journal* 98(2): 29-s to 49-s. DOI: 10.29391/2019.98.003

24. Bai, J. W., Liu, P. P., Zhu, Y. M., Lee, X. M., et al. 2013. Coherent precipitation of copper in Super304H austenite steel. *Materials Science & Engineering A* 584: 57–62. DOI: 10.1016/j.msea.2013.06.082

25. Sawaragi, Y., and Hirano, S. 1991. The development of a new 18-8 austenitic steel (0.1C-18Cr-9Ni-3Cu-Nb,N) with high elevated temperature strength for fossil fired boilers. *Proceedings of the 6th International Conference on Mechanical Behavior of Materials*. ICM.

26. Morales, E. V, ed. 2011. *Alloy Steel — Properties and Use*, 171. London: IntechOpen.

27. Li, X., Zou, Y., Zhang, Z., and Zou, Z. 2010. Microstructure evolution of a novel Super304H steel aged at high temperatures. *Materials Transactions* 51(2): 305–309. DOI: 10.2320/matertrans.MC200916

28. Popov, V. V. 1991. Dissolution of carbides and nitrides during austenitizing of steel. *Metal Science and Heat Treatment* 33: 480–483.

29. Shingledecker, J. 2009. *Strain Induced Precipitation Hardening of Stainless Steels*. Palo Alto: Electric Power Research Institute.

30. Iseda, A., Okada, H., Semba, H., and Igarashi, M. 2008. Long-term creep properties and microstructure of Super 304H, TP347HFG, and HR3C for advanced USC boilers. *Proceedings of the 5th International Conference on Advances in Materials for Fossil Power Plants*, 199–206. ASM International. DOI: 10.1179/174892408X382860

31. Okayasu, M., Fukui, H., and Ohfuji, H. 2013. Strain-induced martensite formation in austenitic stainless steel. *Journal of Materials Science* 48: 6157–6166.

32. Masumura, T., Nakada, N., Tsuchiyama, T., Takaki, S., Koyano, T., and Adachi, K. 2015. The difference in thermal and mechanical stabilities of austenite between carbon- and nitrogen-added metastable austenitic stainless steels. *Acta Materialia* 84: 330–338. DOI: 10.1016/j.actamat.2014.10.041

HAN-SANG LEE (*han1213@kepco.co.kr*) and **BUM-SHIN KIM** are with Korea Electric Power Corp., Daejeon, South Korea. **LEE** and **SUN IG HONG** are with Chungnam National University, Daejeon, South Korea.